Atmos. Chem. Phys. Discuss., 9, 13123–13153, 2009
www.atmos-chem-phys-discuss.net/9/13123/2009/
© Author(s) 2009. This work is distributed under
the Creative Commons Attribution 3.0 License.

Atmospheric Chemistry and Physics Discussions

This discussion paper is/has been under review for the journal *Atmospheric Chemistry and Physics (ACP)*. Please refer to the corresponding final paper in *ACP* if available.

Evidence of the water-cage effect on the photolysis of NO_3^- and $FeOH^{2+}$, and its implications for the photochemistry at the air-water interface of atmospheric droplets

P. Nissenson[1], D. Dabdub[1], R. Das[2,3], V. Maurino[2], C. Minero[2], and D. Vione[2]

[1]Dept. of Mechanical and Aerospace Engineering, University of California, Irvine, CA, USA
[2]Dipartimento di Chimica Analitica, Università degli Studi di Torino, Via P. Giuria 5, 10125 Torino, Italy
[3]Dept. of Chemical Engineering, Haldia Institute of Technology, ICARE complex, Haldia 721657, India

Received: 26 May 2009 – Accepted: 27 May 2009 – Published: 12 June 2009

Correspondence to: D. Vione (davide.vione@unito.it)

Published by Copernicus Publications on behalf of the European Geosciences Union.

Abstract

Experiments are conducted to determine the photolysis quantum yields of nitrate, $FeOH^{2+}$, and H_2O_2 in the bulk and at the surface layer of water. Results show that the quantum yields of nitrate and $FeOH^{2+}$ are enhanced at the surface compared to the bulk due to a reduced water-cage surrounding the photo-fragments ($^{\bullet}OH+^{\bullet}NO_2$ and $Fe^{2+}+^{\bullet}OH$, respectively). However, no evidence is found for an enhanced quantum yield for H_2O_2 at the surface. The photolysis rate constant distribution within nitrate, $FeOH^{2+}$, and H_2O_2 aerosols is calculated by combining the quantum yield data with Mie theory calculations of light intensity. Values for the photolysis rate constant of nitrate and $FeOH^{2+}$ are significantly higher at the surface than in the bulk due to enhanced quantum yields at the surface. The results concerning the rates of photolysis of these photoactive species are applied to the assessment of the reaction between benzene and $^{\bullet}OH$ in the presence of $^{\bullet}OH$ scavengers in an atmospherically relevant scenario. For a droplet of 1 μm radius, a large fraction of the total $^{\bullet}OH$-benzene reaction (15% for H_2O_2, 20% for nitrate, and 35% for $FeOH^{2+}$) occurs in the surface layer, which accounts for just 0.15% of the droplet volume. By neglecting the surface effects on photochemistry, the rate of the important reactions could be underestimated by a considerable amount.

1 Introduction

The photochemical reactions that take place in water droplets may play an important role in atmospheric chemistry, including the formation and transformation of major organic components and pollutants (Jacob, 2000; Harrison et al., 2005a; Vione et al., 2006; Amato et al., 2007). Two major issues arise in studying these photochemical reactions. The first issue is that the actinic flux inside small water droplets can be considerably higher than in the surrounding gas phase, because of refraction and diffraction phenomena (Madronich, 1987). Estimates for the enhancement factor vary from 1.5 to

ACPD

9, 13123–13153, 2009

2 (Nissenson et al., 2006).

The second issue is that some reactions are faster at the air-water interface than in the solution bulk (Hu et al., 1995; Knipping et al., 2000). An interface enhancement also has been observed in the case of the photochemical reactions (Furlan, 1999; Winter and Benjamin, 2004), and a recent study into the photolysis of $Mo(CO)_6$ in 1-decene droplets has provided evidence that a large part of the effect is accounted for by the incomplete cage of the solvent molecules at the interface (Nissenson et al., 2006). In the solution bulk, the fragments that are generated by photolysis are initially surrounded by the cage of the solvent molecules, and their diffusion out of the cage is in competition with regeneration of the photoactive compound through recombination. The effect of the recombination reactions is that of decreasing the photolysis quantum yields in the solution bulk. In the case of $FeCl^{2+}$, recombination processes could decrease the photolysis quantum yield by several orders of magnitude (Khanra et al., 2008). At the interface, the solvent cage is incomplete and the recombination reactions are inhibited as a consequence. The photolysis quantum yields therefore could be higher at the interface than in the bulk. Furthermore, the incomplete cage of water molecules enhances the photochemistry of nitrate in deliquesced mixtures of NaCl and $NaNO_3$ (Wingen et al., 2008).

The quantification of the solvent-cage effect in aqueous solution presents a number of experimental difficulties, which could explain why limited data are available on the topic. In the case of nitrate photolysis that yields $^{\bullet}OH + ^{\bullet}NO_2$, it has been shown that $^{\bullet}OH$ scavengers added to the system at sufficiently elevated concentrations can react with the hydroxyl radical when it is still inside the cage. The result is an enhancement of the generation rate of $^{\bullet}NO_2$, and of the photochemical transformation processes if the reaction intermediates between $^{\bullet}OH$ and the scavenger are themselves reactive (Warneck and Wurzinger, 1988; Bouillon and Miller, 2005; Das et al., 2009).

To our knowledge, no assessment is presently available of the possible impact of the described interface phenomena on the photochemical reactions that take place in water droplets in the atmosphere. This is the purpose of the present paper, in which the effect

of the solvent cage on the photolysis quantum yields of nitrate, $FeOH^{2+}$ and H_2O_2 is studied upon addition of 2-propanol as $^{\bullet}OH$ scavenger. The quantum yields, together with Mie theory calculations for light intensity, are used to calculate the photolysis rate constants of nitrate, $FeOH^{2+}$ and H_2O_2 at atmospherically relevant concentrations inside water droplets illuminated by actinic radiation. The results concerning the rates of photolysis of these photoactive species are applied to the assessment of the reaction between benzene and $^{\bullet}OH$ in the presence of $^{\bullet}OH$ scavengers in an atmospherically relevant scenario.

2 Experimental

$NaNO_3$ (purity grade 99.5%), CCl_4 (for analysis) and acetonitrile (gradient grade) were purchased from VWR Int., $NaNO_2$ (97+%), $Fe(ClO_4)_3$ (low chloride), H_2O_2 (35%), HCl (37%), $HClO_4$ (70%), H_3PO_4 (85%), 1,10-phenanthroline monohydrate (99%) and 2,4-dinitrophenylhydrazine (97%) from Aldrich, $FeSO_4{\cdot}7\,H_2O$ (99%) from Carlo Erba, acetone (for residue analysis) from Fluka, 2-propanol (LC-MS Chromasolv) from Riedel-de Haën. All reagents were used as received, without further purification.

Samples to be irradiated (5 mL total volume) are placed in Pyrex glass cells (4.0 cm diameter, 2.3 cm height), and magnetically stirred during irradiation. Irradiation is carried out under UV lamps, of which one with an emission maximum at 313 nm (Philips TL 01) and 5.6 $W\,m^{-2}$ irradiance, measured with a CO.FO.ME.GRA. (Milan, Italy) power meter, and corresponding to 3.7×10^{-6} einstein $L^{-1}\,s^{-1}$ in solution. The other lamp (Philips TLK05) has an emission maximum at 365 nm and 5.5 $W\,m^{-2}$ irradiance, corresponding to 4.2×10^{-6} einstein $L^{-1}\,s^{-1}$ in solution. The absorption spectra of nitrate, hydrogen peroxide and Fe(III), the latter at pH 2.5, taken with a Varian Cary 100 Scan UV-Vis spectrophotometer, are reported in Fig. 1.

The determination of acetone formation from 2-propanol is carried out by pre-column derivatization with 2,4-dinitrophenylhydrazine (10 min contact time; Warneck and Wurzinger, 1988), followed by analysis of the resulting hydrazone with High

ACPD
9, 13123–13153, 2009

Performance Liquid Chromatography coupled with Diode Array Detection (HPLC-DAD). Nitrite is also determined by derivatization with 2,4-dinitrophenylhydrazine (10 min contact time; Kieber and Seaton, 1996), followed by HPLC-DAD determination of the azide formed. It is necessary to subject the stock phenylhydrazine solution to extraction with CCl_4, in order to remove the azide contamination caused by the reaction with ambient nitrogen dioxide (Kieber and Seaton, 1996). The adopted instrument is a LaChrom ELITE VWR-Hitachi HPLC-DAD, equipped with L-2200 autosampler, L-2130 pump for low-pressure gradients, L-2300 column oven, L-2455 DAD detector, and a column Merck LiChroCART 125-4 (125 mm length by 4 mm diameter), packed with LiChrospher 100 RP18 (particle diameter 5 μm). Isocratic elution is performed with a 50:50 mixture of acetonitrile and aqueous H_3PO_4 (pH 2.8), at 1.00 mL min^{-1} flow rate. The retention time (t_R, min) and quantification wavelength (λ, nm) are as follows (t_R, λ): nitrite (3.3, 307), acetone (6.8, 368).

Fe^{2+} is determined with a Varian Cary 100 Scan UV-Vis spectrophotometer, as complex with 1,10-phenanthroline (absorption maximum at 510 nm) (Calvert and Pitts, 1966).

The time evolution data of nitrite and acetone are fitted with equations of the form $[I]_t = k_I^f [S]_0 (k_I^d - k_S^d)^{-1} [\exp(-k_S^d t) - \exp(-k_I^d t)]$, where $[I]_t$ is the concentration of the intermediate (nitrite or acetone) at the time t, $[S]_0$ the initial concentration of the substrate (nitrate or 2-propanol), k_I^f and k_I^d the pseudo-first order rate constants for the formation and degradation of the intermediate, and k_S^d the pseudo-first order rate constant for the degradation of the substrate. The initial formation rate of the intermediate is given by $R_I = k_I^f [S]_0$. The error bounds associated to the rate data represent $\mu \pm \sigma$, derived from the fit of the theoretical curves to the experimental data (intra-series variability). The reproducibility of repeated runs (inter-series variability) is approximately 10–15%.

ACPD
9, 13123–13153, 2009

3 Results and discussion

3.1 Water-cage effect on the photolysis quantum yields

Figure 2 reports the initial formation rates of nitrite and acetone ($(CH_3)_2CO$) upon UVB irradiation of 0.01 M $NaNO_3$, as a function of the concentration of 2-propanol ($(CH_3)_2CHOH$). The following processes account for the formation of nitrite and acetone in the system (Warneck and Wurzinger, 1988; Mark et al., 1996):

$$NO_3^- + h\nu + H^+ \rightleftarrows [^\bullet OH + ^\bullet NO_2]_{cage} \rightarrow \quad ^\bullet OH + ^\bullet NO_2 \tag{1}$$

$$NO_3^- + h\nu \rightarrow NO_2^- + O \tag{2}$$

$$2\,^\bullet NO_2 \rightleftarrows N_2O_4 \tag{3}$$

$$N_2O_4 + H_2O \rightarrow NO_3^- + NO_2^- + 2H^+ \tag{4}$$

$$O + NO_3^- \rightarrow O_2 + NO_2^- \tag{5}$$

$$(CH_3)_2CHOH + ^\bullet OH \rightarrow (CH_3)_2C^\bullet OH + H_2O \text{ or other intermediates} \tag{6}$$

$$(CH_3)_2C^\bullet OH + O_2 \rightarrow (CH_3)_2CO + HO_2^\bullet \tag{7}$$

$$(CH_3)_2CHOH + O \rightarrow (CH_3)_2C^\bullet OH + ^\bullet OH \text{ or } (CH_3)_2CO + H_2O \tag{8}$$

At elevated [2-propanol], the reaction between the alcohol and $^\bullet OH$ inside the water cage could reduce the in-cage recombination between $^\bullet OH$ and $^\bullet NO_2$, enhancing as a consequence the formation of both acetone and nitrite. The possibility for $^\bullet OH$ scavengers to react with the hydroxyl radical inside the solvent cage, with an overall enhancement of nitrate photochemistry already has been demonstrated in the case of bromide (Das et al., 2009). The work of Warneck and Wurzinger (1988) has shown that the kinetics of acetone formation can be accounted for better than the formation

ACPD
9, 13123–13153, 2009

of nitrite by the known processes of nitrate photolysis. This is probably due to the presence of unaccounted, additional processes that yield nitrite (Mark et al., 1996). The formation rate of acetone is therefore a better measure of the quantum yield of $^{\bullet}$OH photoproduction, $\Phi(^{\bullet}OH)$. It has been shown that $\Phi(^{\bullet}OH)=1.15\Phi(\text{Acetone})$ (Warneck and Wurzinger, 1988). Note that $\Phi(\text{acetone})=R_{\text{Acetone}}\,(P_{a,NO_3^-})^{-1}$, where R_{Acetone} is the measured initial formation rate of acetone, and P_{a,NO_3^-} is the photon flux absorbed by nitrate. By application of the Lambert-Beer law one gets $P_{a,NO_3^-}=6\times10^{-8}$ einstein L^{-1} s^{-1} for 0.01 M NO_3^-.

This study finds $\Phi(^{\bullet}OH)\approx0.01$ at low [2-propanol], in agreement with previous literature reports (Warneck and Wurzinger, 1988), and $\Phi(^{\bullet}OH)=0.034$ at elevated [2-propanol], which would be consistent with a reaction between 2-propanol and cage $^{\bullet}$OH. Interestingly, the value of $\Phi(^{\bullet}OH)$ found by this study upon irradiation with maximum at 313 nm is similar to the result of Warneck and Wurzinger (1988) at 305 nm, in agreement with previous reports that the quantum yield of $^{\bullet}$OH generation upon nitrate photolysis is independent of the irradiation wavelength (Mark et al., 1996; Mack and Bolton, 1999).

Figure 3 reports the initial formation rate of acetone for different concentration values of 2-propanol, upon irradiation of 0.1 mM $Fe(ClO_4)_3$ at pH 2.5, where the most important photoactive species of Fe(III) is $FeOH^{2+}$ (Mazellier et al., 1997).

$$FeOH^{2+} + h\nu \rightleftarrows [Fe^{2+} +^{\bullet} OH]_{cage} \rightarrow Fe^{2+} +^{\bullet} OH \quad (9)$$

Considering that Fe(III) cannot scavenge $^{\bullet}$OH, 2-propanol would be the only species able to react with the hydroxyl radicals at the beginning of the reaction. Fe^{2+} can react with $^{\bullet}$OH, but the reaction rate constant is not extremely high (4.3×10^8 M^{-1} s^{-1}; Buxton et al., 1988) and the compound is not present in the system from the beginning. Therefore, Fe^{2+} has to be accumulated before being able to compete effectively for $^{\bullet}$OH. The determination of Fe(II) as a function of the irradiation time shows that its concentration was always below 20 μM, and not higher than 10 μM at short irradiation time. Considering that the reaction rate constant between 2-propanol and $^{\bullet}$OH is around 4.5 times

higher than that of Fe^{2+}, the ferrous ion would have a minor to negligible impact on the initial formation rate of acetone above 10^{-5} M 2-propanol. Under such conditions, with 2-propanol as the major $^{\bullet}OH$ scavenger one would expect the formation rate of acetone to reach a plateau quickly in the absence of the solvent-cage effect. The increase of the initial formation rate of acetone with increasing [2-propanol] provides evidence of a reaction between the alcohol and $^{\bullet}OH$ inside the cage of the water molecules. By reacting with $^{\bullet}OH$ inside the cage, 2-propanol would inhibit the cage recombination between Fe^{2+} and $^{\bullet}OH$ and enhance the formation of acetone.

Interestingly, the formation rate of acetone is considerably higher under UVB irradiation (emission maximum at 313 nm) than under UVA (emission maximum at 365 nm). The formation of acetone from 2-propanol would be a direct measurement of the $^{\bullet}OH$ yield from $FeOH^{2+}$, considering that Eq. (9) would be the main process under irradiation because Fe^{3+} is poorly photoactive (Benkelberg and Warneck, 1995; Mazellier et al., 1997). $FeOH^{2+}$ also would be the main absorbing species in the relevant wavelength interval (Benkelberg and Warneck, 1995). From $\Phi(^{\bullet}OH)=R_{Acetone}\,(P_{a,Fe(III)})^{-1}$ it is possible to derive $\Phi(^{\bullet}OH)$ = 0.14 (low [2-propanol]) and $\Phi(^{\bullet}OH)\approx1$ (high propanol) under UVB (emission maximum at 313 nm), and $\Phi(^{\bullet}OH)$ = 0.04 (low propanol) and $\Phi(^{\bullet}OH)$=0.18 (high propanol) under UVA (emission maximum at 365 nm). Note that from the Lambert-Beer law $P_{a,Fe(III)}=6\times10^{-8}$ einstein L^{-1} s^{-1} is obtained under UVB, and $P_{a,Fe(III)}=3\times10^{-8}$ einstein L^{-1} s^{-1} under UVA irradiation. The quantum yields measured at low [2-propanol] are in good agreement with those reported by Benkelberg and Warneck (1995).

Figure 4 reports the formation rate of acetone upon UVB irradiation of 0.01 M H_2O_2, as a function of [2-propanol]. Hydrogen peroxide yields $^{\bullet}OH$ upon irradiation, and a photolysis quantum yield of 0.5 has been reported in the aqueous solution. Considering that the photolysis quantum yield of gaseous H_2O_2 is around 1 (Finlayson-Pitts and Pitts, 1986), and that a solvent cage is not present in the gas phase, there is a reasonable possibility that the cage of the water molecules inhibits the photolysis of H_2O_2 in solution. Unlike nitrate and Fe(III), H_2O_2 can scavenge as well as produce

$^{\bullet}$OH. Accordingly, the competition for reaction with $^{\bullet}$OH between 2-propanol (Eq. 6, rate constant $1.9\times10^{9}\,M^{-1}\,s^{-1}$; Buxton et al., 1988) and H_2O_2 (Eq. 11, rate constant $2.7\times10^{7}\,M^{-1}\,s^{-1}$; Buxton et al., 1988) has to be considered.

$$H_2O_2 + h\nu \rightleftarrows [2^{\bullet}OH]_{cage} \rightarrow 2^{\bullet}OH \quad (10)$$

$$H_2O_2 + {}^{\bullet}OH \rightarrow HO_2^{\bullet} + H_2O \quad (11)$$

The observed increase of the formation rate of acetone with [2-propanol] could be due to the reaction between the alcohol and $^{\bullet}$OH when the latter is still inside the solvent cage. However, the increase would be caused at least in part by a better competition for $^{\bullet}$OH of 2-propanol when the alcohol is more concentrated. It is possible to assess the effect of such a competition by considering Eqs. (10, 11, 6), and by hypothesizing a constant production rate of $^{\bullet}$OH, $R_{^{\bullet}OH}$, in Eq. (10). In this way one would account for the reaction between $^{\bullet}$OH and 2-propanol or H_2O_2, but not for the solvent-cage effect. Upon application of the steady-state approximation to $^{\bullet}$OH one gets Eq. (12):

$$\left(\frac{d[\mathrm{Acetone}]}{dt}\right)_{t\rightarrow 0} = \frac{R_{^{\bullet}OH}\cdot k_6\cdot[2-\mathrm{Propanol}]}{k_6\cdot[2-\mathrm{Propanol}] + k_{11}\cdot[H_2O_2]} \quad (12)$$

Equation (12) is superposed to the experimental data in Fig. 4, and it reproduces quite well the observed experimental trend. Accordingly, it is not strictly necessary to hypothesize a reaction between 2-propanol and cage $^{\bullet}$OH in the case of H_2O_2. Although the possibility is reasonable given the difference between the photolysis quantum yields of H_2O_2 in the gas phase and in aqueous solution, no evidence for such an effect could be derived from the present experimental data.

3.2 Radiation absorption calculations inside small, spherical water droplets

Photolysis rate constants are functions of absorber quantum yield, absorber molar absorption coefficient (ε), and the light spectrum. These parameters, in turn, may be

ACPD
9, 13123–13153, 2009

functions of wavelength and/or location (for example, bulk versus surface layer). Objects with curved surfaces, such as spherical water droplets, may refract light and create peaks and troughs of light intensity within the object (Bohren and Huffman, 1983; Barber and Hill, 1990). In order to calculate the rate of photolysis within small, spherical droplets, it is necessary to calculate the intensity distribution within the droplets. In the atmosphere, many droplets are similar in size to the wavelength of the incident light and the wave picture of light must be used to calculate the internal intensity distribution (Bohren and Huffman, 1983; Barber and Hill, 1990). This approach, known as Mie theory, has been used in numerous studies to show that the internal intensity distribution is non-uniform and may be enhanced by several orders of magnitude in certain locations due to morphology-dependent resonances, or MDRs (Bohren and Huffman, 1983; Chylek et al., 1985; Benincasa et al., 1987; Barber and Hill, 1990; Ray and Bhanti, 1997; Ruggaber et al., 1997; Mayer and Madronich, 2004; Nissenson et al., 2006).

The numerical model used to calculate the internal intensity distribution is described in Nissenson et al. (2006). Briefly, the light spectrum is discretized into many individual polarized plane-waves which are incident upon an isotropic and homogenous (with respect to angle) spherical water droplet containing absorbers. Careful attention is given to the discretization size so that all MDRs are accounted for. The intensity at a given point within the droplet relative to the incident intensity is,

$$I^{\mathrm{drop,rel}}(\lambda, m, r/a, \theta, \phi) = \frac{mE(m, r/a, \theta, \phi)E^{*}(m, r/a, \theta, \phi)}{E_0^2} \quad (13)$$

where r, θ, and ϕ are the spherical coordinates, λ is the wavelength, m is the index of refraction, a is the droplet radius, E is the electric field, E^* is the complex conjugate of the electric field, and E_0^2 is the incident intensity. The electric field is expressed as an infinite series of vector spherical harmonics and sufficient terms are summed over until convergence is reached.

Droplets in the atmosphere are illuminated non-uniformly over direction. Therefore

ACPD
9, 13123–13153, 2009

a useful quantity is the angle-averaged relative intensity distribution as a function of normalized radius since it is independent of the direction of illumination,

$$I_{\mathrm{ang}}^{\mathrm{drop,rel}}(\lambda, m, r/a = \frac{\frac{1}{4\pi}\int_0^{2\pi}\int_0^{\pi} mE \bullet E^* \sin\theta d\theta d\phi}{E_0^2}, \quad (14)$$

where the subscript ang refers to the angle-averaged relative intensity. At each radial shell, $I_{\mathrm{ang}}^{\mathrm{drop,rel}}(\lambda, m, r/a)$ is calculated for every wavelength. Averaging over all wavelengths yields the angle- and wavelength-averaged intensity distribution as a function of normalized radius,

$$I_{\mathrm{ang},\lambda}^{\mathrm{drop,rel}}(r/a) = \frac{1}{N}\sum_{\lambda} I_{\mathrm{ang}}^{\mathrm{drop,rel}}(m, \lambda, r/a)W(\lambda), \quad (15)$$

where N is the number of discretizations of the wavelength range and $W(\lambda)$ is a weighting factor that accounts for the actinic flux being a function of wavelength.

The photolysis rate constant of a photoactive species S, $J_P^S(r/a, \theta, \phi)$, is a function of the intensity distribution and therefore is non-uniform throughout the droplet. The angle-averaged photolysis rate constant, $J_P^S(r/a)$, is calculated using $I_{\mathrm{ang}}^{\mathrm{drop,rel}}(m, \lambda, r/a)$ in a manner similar to Ray and Bhanti (1997),

$$J_P^S(r/a) = \sum_{\lambda} G(\lambda)\Phi(\lambda, r/a)\sigma(\lambda)I_{\mathrm{ang}}^{\mathrm{drop,rel}}(m, \lambda, r/a)\Delta(\lambda), \quad (16)$$

where $G(\lambda)$ is the spectral flux (in units of photons $\mathrm{cm}^{-2}\,\mathrm{s}^{-1}\,\mathrm{nm}^{-1}$). $G(\lambda)$ is multiplied by $I_{\mathrm{ang}}^{\mathrm{drop,rel}}(m, \lambda, r/a)$, which is a measure of the actinic flux enhancement at a particular wavelength.

The index of refraction of the droplet is a function of wavelength and radius, and contains a real and imaginary part. Since the solutes are present in very low concentrations (10^{-4} M or less), the real part of the index of refraction (m_r) of the solvent is assumed to be that of water and is calculated using the formula of Quan and

ACPD
9, 13123–13153, 2009

Fry (1995). The imaginary part of the index of refraction of the droplet (m_i) determines the absorbance of the solution and is calculated in the same manner as Ray and Bhanti (1997),

$$m_i(\lambda, r/a) = m_{i,0}(\lambda) + \frac{\overline{n}(r)\Phi(\lambda, r/a)\sigma(\lambda)\lambda}{4\pi} N_a, \quad (17)$$

where $m_{i,0}(\lambda)$ is the imaginary index of refraction of pure water (taken from Hale and Querry, 1973), $\overline{n}(r)$ is the concentration of the absorber, $\Phi(\lambda, r)$ is the quantum yield of the absorber, $\sigma(\lambda)$ is the absorption cross section of the absorber, and N_a is Avogadro's number.

Two different actinic flux spectra are used to calculate the light intensity distribution inside a water droplet. The first spectrum is from Frank and Klöpffer (1988), which is the actinic flux measured over the Central Europe (52° N) during 15 June averaged from 8 a.m. to 4 p.m. The second spectrum is from Finlayson-Pitts and Pitts (2000), which is the theoretical actinic flux value for a solar zenith angle of 30° and a surface albedo of 80%. The spectrum in Finlayson-Pitts and Pitts (2000) also is used in Nissenson et al. (2006).

In the case of nitrate, a concentration of 10^{-4} M is adopted which is typical of continental clouds (Warneck, 1999). It has been reported that NO_3^- has some limited tendency to undergo surface accumulation (Salvador et al., 2003; Vacha et al., 2006), but not so much as to increase significantly the concentration of nitrate at the air-water interface compared to the bulk. For this reason, the concentration of nitrate is assumed constant through the whole volume of the droplet. Based on the experimental data described before, the photolysis quantum yield adopted for nitrate is 0.01 in the bulk and 0.034 at the surface. As with $FeOH^{2+}$ and H_2O_2, a surface layer of 0.5 nm thickness is adopted for nitrate, which would make up 0.15% of the volume of a spherical droplet with 1 μm radius. An interface thickness of approximately five atomic lengths is consistent with molecular dynamics simulations (Winter and Benjamin, 2004; Jungwirth and Tobias, 2006).

ACPD
9, 13123–13153, 2009

In the case of $FeOH^{2+}$ the adopted concentration is 10^{-6} M (Warneck, 1999). Although in principle it is possible that the concentration of the Fe(III) ions is lower at the surface than in the bulk, no data of the bulk-to-surface profile are available. Accordingly, a constant concentration is assumed throughout the droplet. The photolysis quantum yield of $FeOH^{2+}$ varies with wavelength, and the wavelength trend is known in the bulk (Benkelberg and Warneck, 1995). Table 1 reports the photolysis quantum yields of $FeOH^{2+}$ adopted here in the case of the bulk (based on data from Benkelberg and Warneck, 1995) and the surface layer (reduced or absent solvent-cage effect). In the latter case the experimental data are available for 313 and 365 nm. The values at the other wavelengths are derived by assuming that a similar wavelength trend is operational for the photolysis quantum yield of $FeOH^{2+}$, in the absence and in the presence of the solvent-cage effect.

Hydrogen peroxide is present in continental clouds at 10^{-5} M levels (Warneck, 1999). It has some affinity for the air-water interface, and it has been reported that its interface concentration could be double compared to the bulk (Vacha et al., 2004). Accordingly, the adopted concentration values are 1×10^{-5} M in the solution bulk, and 2×10^{-5} M at the surface. The adopted value for the photolysis quantum yield of H_2O_2 is 0.5 (Finlayson-Pitts and Pitts, 1986), both in the bulk and at the surface.

Figure 5 presents calculations for $I_{\mathrm{ang}}^{\mathrm{drop,rel}}(r/a)$ using the spectrum from Finlayson-Pitts and Pitts (2000) and the resulting $J_P^{NO_3^-}(r/a)$ for nitrate droplets of three different sizes. The value of $I_{\mathrm{ang}}^{\mathrm{drop,rel}}(r/a)$ and $J_P^{NO_3^-}(r/a)$ vary little throughout most of the bulk. Near the surface (r/a=1), $I_{\mathrm{ang}}^{\mathrm{drop,rel}}(r/a)$ decreases causing $J_P^{NO_3^-}(r/a)$ to decrease as well. However, at the surface layer $J_P^{NO_3^-}(r/a)$ increases sharply due to enhanced quantum yields for nitrate in that region. Similar results are observed for $FeOH^{2+}$ aerosols as this species also has enhanced quantum yields at the surface. For H_2O_2 aerosols, the value of $J_P^{H_2O_2}(r/a)$ at the surface is reduced compared to the bulk because the

ACPD
9, 13123–13153, 2009

quantum yield of H_2O_2 is assumed constant throughout the aerosol.

3.3 Assessment of the reaction rate between benzene and •OH

Benzene is chosen as a model aromatic substrate that can undergo accumulation at the air-water interface of atmospheric droplets. There are different estimates for the possible extent of the surface concentration of benzene compared to the bulk (Vacha et al., 2006; Vione et al., 2007), and here an accumulation factor of 75 is assumed. Such a value is not uncommon for aromatic compounds in atmospheric waters (Minofar et al., 2007), the bulk concentrations of which are often in the nM range (Harrison et al., 2005b). The adopted concentrations of benzene are 10^{-8} M in the bulk and 7.5×10^{-7} M at the interface. For simplicity issues, the same thickness of the surface layer as already adopted for the photolysis quantum yields (0.5 nm) also is used for benzene accumulation. Another reason for the choice of benzene is that this compound reacts very selectively with •OH, and can be used as a probe of •OH photoproduction in surface and atmospheric waters (Anastasio and McGregor, 2001; Takeda et al., 2004).

Atmospheric water droplets contain a wide variety of organic compounds that can act as •OH scavengers and, therefore, could compete with the chosen model molecule for the reaction with the hydroxyl radical. Among the known droplet components, formate prevails as •OH scavenger (Minero et al., 2007) because of its relatively elevated concentration (typical values for cloud water are around 10^{-5} M; Marinoni et al., 2004) and reaction rate constant ($k_{HCOO^-/•OH}=3.2\times10^9\ M^{-1}\ s^{-1}$; Buxton et al., 1988). Formate could account for around one half of the total scavenging of •OH in typical continental clouds (Minero et al., 2007), and should be present at about equal concentration in the solution bulk and at the interface (Minofar et al., 2007). For simplicity, here the •OH scavengers in water droplets are assumed to be equivalent to 2×10^{-5} M formate, and to follow its same distribution within the droplet. The latter assumption is justified by the fact that the most common •OH scavengers in cloud water are short-chain carboxylic and bicarboxylic acids (Marinoni et al., 2004; Minero et al., 2007). Let J_P^S be the photolysis rate constant of the compound S (NO_3^-, $FeOH^{2+}$ or H_2O_2)

ACPD
9, 13123–13153, 2009

to yield $^{\bullet}$OH, [S] its concentration at the droplet surface or in the bulk, [Benzene] and [Scav] the corresponding concentration values of benzene and the $^{\bullet}$OH scavengers, respectively ([Scav]=2×10^{-5} M in the whole droplet), k_{scav}=3.2×10^{9} M^{-1} s^{-1} and k_B=7.8×10^{9} M^{-1} s^{-1} (Buxton et al., 1988) the respective second-order rate constants for reaction with $^{\bullet}$OH. J_P^S is calculated in the same manner as $J_P^S(r/a)$ above. The reaction rate between benzene and $^{\bullet}$OH (Rate$_{B/^{\bullet}OH}$), in competition with the $^{\bullet}$OH scavengers, would be expressed as follows:

$$\text{Rate}_{B/^{\bullet}OH} = J_P^S \cdot [S] \cdot \frac{k_B \cdot [\text{Benzene}]}{k_B \cdot [\text{Benzene}] + k_{scav} \cdot [\text{Scav}]} \quad (18)$$

Among the variables of Eq. (18), $J_P(S)$, [S] and [Benzene] can vary depending on the position inside the droplet (bulk or surface layer). The surface thickness is assumed to be 0.5 nm, equal for all the processes (benzene and H_2O_2 accumulation, interface enhancement of the photolysis quantum yields). Equation (18) reports the reaction rate of benzene in a certain point of the droplet, depending on the local values of the relevant variables. Because of the spherical symmetry, the variations are expected to occur as a function of the distance from the droplet center. The latter will be expressed here as r/a that varies from 0 to 1, where 0 represents the center and 1 the surface. Rate$_{B/^{\bullet}OH}$ is expressed in mol L^{-1} s^{-1}. To obtain the number of moles of benzene transformed per unit time in the whole droplet or in a part of it, one has to integrate over the volume. Let $F(r/a)$ be the ratio between the number of moles of benzene transformed per unit time inside the spherical section of radius r/a, and the total number of moles transformed inside the whole droplet (r/a=1). Following this definition, $F(r/a)$ can be expressed as follows (Rate$_{B/^{\bullet}OH}$ is expressed by Eq. (18) and is a function of r/a, because in

general J_P^S, [S] and [Benzene] all depend on r/a):

$$F(r/a) = \frac{\int_o^{r/a} \left[\text{Rate}_{B/\bullet OH}(r/a)\right] \cdot [r/a]^2 \, d(r/a)}{\int_o^{1} \left[\text{Rate}_{B/\bullet OH}(r/a)\right] \cdot [r/a]^2 \, d(r/a)} \quad (19)$$

Numerical integration was carried out whenever relevant. Figure 6 reports the trends of $\text{Rate}_{B/\bullet OH}(r/a)$ and $F(r/a)$ vs. r/a in the case of 10^{-4} M nitrate. The data are reported for different values of the droplet radius, a=1, 2 and 3 μm. Figure 6a is based on the sunlight spectrum reported by Finlayson-Pitts and Pitts (2000), Fig. 6b on the spectrum of Frank and Klöpffer (1988). Note that $\text{Rate}_{B/\bullet OH}$ differs by about one order of magnitude in the two cases, while the F(r/a) curves are very similar. The distribution of the reaction within the droplet volume, of which $F(r/a)$ is a measurement, varies very little with the intensity of sunlight. Also note that the trend of $F(r/a)$ vs. r/a shows a continuous increase, followed by a sudden jump to reach $F(r/a)$=1 very near the droplet surface. That "jump" is the contribution of the surface layer to the reaction.

The corresponding plots for 10^{-6} M $FeOH^{2+}$ and 10^{-5} M H_2O_2 are reported in Figs. 7 and 8, respectively. In the case of the droplets with 1 μm radius, a considerable fraction of the total reaction takes place in a surface layer that accounts for just 0.15% of the droplet volume. Such a fraction is around 20% for NO_3^-, 35% for $FeOH^{2+}$, and 15% for H_2O_2. Note that the adopted surface accumulation of benzene is the same in all the cases, thus the differences are linked to the water-cage effect on the photolysis quantum yields of nitrate and $FeOH^{2+}$, and to the surface accumulation for H_2O_2. For larger droplets the surface layer accounts for a lower fraction of the total volume, and its relative contribution to the overall reaction is lower. Also note that the values of $\text{Rate}_{B/\bullet OH}$ under equal conditions of sunlight illumination are in the order $FeOH^{2+} > NO_3^- > H_2O_2$, and that $FeOH^{2+}$ would therefore be the main source of $^\bullet$OH inside a typical droplet. The role of the surface layer toward the transformation of benzene would therefore

ACPD
9, 13123–13153, 2009

reflect more closely that calculated in the case of $FeOH^{2+}$, at least for very short reaction times.

4 Conclusions

Evidence is found for an effect of the cage of the water molecules on the photolysis quantum yields of nitrate and $FeOH^{2+}$. The photo-fragments ($^{\bullet}OH+^{\bullet}NO_2$ in the former case, $Fe^{2+}+^{\bullet}OH$ in the latter) in aqueous solution would initially be surrounded by the cage of the solvent molecules, which would enhance the recombination processes. If the solvent cage is absent or incomplete, as can happen at the air-water interface of disperse droplets, the recombination processes would be inhibited and the effective photolysis quantum yields would be increased accordingly. It was assessed here that the water-cage effect would decrease by 3.4 times the quantum yield of nitrate photolysis, and by 4 to 7 times the photolysis quantum yield of $FeOH^{2+}$, depending on the wavelength range (UVA or UVB). The rate of the relevant photochemical reactions at the air-water interface could be increased by similar ratios compared to the bulk. In the case of H_2O_2, no evidence was obtained of a solvent-cage effect on the photolysis quantum yield. However, H_2O_2 would undergo surface accumulation (Vacha et al., 2004) that could enhance photochemistry.

An important consideration is that the light intensity available to photolyze the dissolved compounds is influenced by the droplet geometry, and that it varies within the droplet volume. Mie theory calculations show that the internal light intensity is enhanced relative to the incident light intensity, with the enhancement lower near the surface compared to the interior. However, the rate of photolysis is significantly higher in the surface layer (0.5 nm thickness) than in the rest of the droplet due to higher quantum yields or surface accumulation, as seen for instance in Fig. 5.

The results concerning the rates of photolysis of 100 μM NO_3^-, 1 μM $FeOH^{2+}$, and 10 μM H_2O_2, as a function of the distance from the droplet center, are applied to the assessment of the reaction between 10 nM benzene and $^{\bullet}OH$, in the presence of a

ACPD
9, 13123–13153, 2009

homogeneous distribution of $^{\bullet}$OH scavengers equivalent to 20 μM formate. Calculations are performed for droplets of 1, 2 and 3 μm radius. In the case of 1 μm, the results show that in the surface layer (0.5 nm thickness, accounting for 0.15% of the total volume) it would take place around 15–35% of the total droplet reaction. The highest figure is that of $FeOH^{2+}$, which is also the most photoactive species at the adopted concentration values that are typical of continental clouds (Warneck, 1999). However, an important limit concerning the photochemistry of $FeOH^{2+}$ in cloud water is represented by its short lifetime under irradiation, of about 30 s (Warneck, 1999). From Figure 7a one obtains $Rate_{B/^{\bullet}OH} \approx 10^{-9}\,M\,s^{-1}$ for 7.5×10^{-7} M benzene in the surface layer, which under a pseudo-first order kinetics would mean transformation of about 5% benzene in 30 s because of $FeOH^{2+}$ photolysis.

Nitrate is a longer-lived species (Warneck, 1999), and some 20% of the total reaction that would occur in a 1 μm droplet takes place in the surface layer. That percentage would also be the error that one would make in the assessment of the nitrate-induced photochemistry by neglecting the surface reactivity. In the case of larger droplets the volume fraction of the surface layer decreases, and the relative importance of the interface photochemistry decreases as well. However, the surface layer would still make a very significant contribution to the overall reaction.

Acknowledgements. DV, VM and CM acknowledge financial support by MIUR-PRIN 2007 (2007L8Y4NB, Area 02, project no. 36), PNRA – Progetto Antartide and Università di Torino – Ricerca Locale. The bursary of RD in Torino was supported by MIUR – Progetto India and by Compagnia di San Paolo. In addition, PN and DD acknowledge financial support by the United States National Science Foundation (Grant Nos. CHE-0431312 and ATM-0423804).

References

Amato, P., Demeer, F., Melahoui, A., Fontanella, S., Martin-Biesse, A. S., Sancelme, M., Laj, P., and Delort, A. M.: A fate for organic acids, formaldehyde and methanol in cloud water: their

biotransformation by microorganisms, Atmos. Chem. Phys., 7, 4159–4169, 2007, http://www.atmos-chem-phys.net/7/4159/2007/.
Anastasio, C. and McGregor, K. G.: Chemistry of fog waters in California's Central Valley: 1. In situ photoformation of hydroxyl radical and singlet molecular oxygen, Atmos. Environ., 35, 1079–1089, 2001.
Barber, P. W. and Hill, S. C.: Light Scattering by Particles: Computational Methods, World Scientific, Singapore, 1990.
Benincasa, D. S., Barber, P. W., Zhang, J., Hsieh, W., and Chang, R. K.: Spatial distribution of the internal and near-field intensities of large cylindrical and spherical scatters, Appl. Opt., 26, 1348–1356, 1987.
Benkelberg, H.-J. and Warneck, P.: Photodecomposition of iron(III) hydroxo and sulfato complexes in aqueous solution: Wavelength dependence of OH and SO_4^- quantum yields, J. Phys. Chem., 99, 5214–5221, 1995.
Bohren, C. F. and Huffman, D. R.: Absorption and Scattering of Light by Small Particles, Wiley, New York, 1983.
Bouillon, R. C. and Miller, W. L.: Photodegradation of dimethyl sulfide (DMS) in natural waters: laboratory assessment of the nitrate-photolysis-induced DMS oxidation, Environ. Sci. Technol., 39, 9471–9477, 2005.
Buxton, G. V., Greenstock, C. L., Helman, W. P., and Ross, A. B.: Critical review of rate constants for reactions of hydrated electrons, hydrogen atoms and hydroxyl radicals ($^\bullet OH/^\bullet O^-$) in aqueous solution, J. Phys. Chem. Ref. Data, 17, 1027–1284, 1988.
Calvert, J. G. and Pitts, J. R.: Photochemistry, Wiley, NY, 1966.
Chylek, P., Pendleton, J. D., and Pinnick, R. G.: Internal and near-surface scattered field of a spherical particle at resonant conditions, Appl. Opt., 24, 3940–3942, 1985.
Das, R., Dutta, B. K., Maurino, V., Vione, D., and Minero, C.: Suppression of inhibition of substrate photodegradation by scavengers of hydroxyl radicals: the solvent-cage effect of bromide on nitrate photolysis, Environ. Chem. Lett., doi:10.1007/s10311-008-0176-8, in press, 2009.
Finlayson-Pitts, B. J. and Pitts Jr., J. R.: Atmospheric Chemistry, Wiley, NY, 1986.
Frank, R. and Klöpffer, W.: Spectral solar photon irradiance in Central Europe and the adjacent North Sea, Chemosphere, 17, 985–994, 1988.
Furlan, A.: Photodissociation of surface-active species at a liquid surface: a study by time-of-flight spectroscopy, J. Phys. Chem. B., 103, 1550–1557, 1999.

ACPD
9, 13123–13153, 2009

Hale, G. M. and Querry, M. R.: Optical constants of water in the 200-nm to 200-micrometer wavelength region, Appl. Opt., 12, 555–563, 1973.
Harrison, M. A. J., Healk, M. R., and Cape, J. N.: Evaluation of the pathways of tropospheric nitrophenol formation from benzene and phenol using a multiphase model, Atmos. Chem. Phys., 5, 1679–1695, 2005a, http://www.atmos-chem-phys.net/5/1679/2005/.
Harrison, M. A. J., Barra, S., Borghesi, D., Vione, D., Arsene, C., and Olariu, R. I.: Nitrated phenols in the atmosphere: A review, Atmos. Environ., 39, 231–248, 2005b.
Hu, J., Shi, Q., Davidovits, P., Worsnop, D. R., Zahniser, M. S., and Kolb, C. E.: Reactive uptake of Cl_2(g) and Br_2(g) by aqueous surfaces as a function of $Br^-$and I^- ion concentration – The effect of chemical reaction at the interface, J. Phys. Chem., 99, 8768–8776, 1995.
Jacob, D.: Heterogeneous chemistry and tropospheric ozone, Atmos. Environ., 34, 2131–2159, 2000.
Jungwirth, P. and Tobias, D. J.: Specific ion effects at the air/water interface, Chem. Rev., 106, 1259–1281, 2006.
Khanra, S., Minero, C., Maurino, V., Pelizzetti, E., Dutta, B. K., and Vione, D.: Phenol transformation induced by UVA photolysis of the complex $FeCl^{2+}$, Environ. Chem. Lett., 6, 29–34, 2008.
Kieber, R. J. and Seaton, P. J.: Determination of subnanomolar concentrations of nitrite in natural waters, Anal. Chem., 67, 3261–3264, 1996.
Knipping, E. M., Lakin, M. J., Foster, K. L., Jungwirth, P., Tobias, D. J., Gerber, R. B., Dabdub, D., and Finlayson-Pitts, B. J.: Experiments and simulations of ion-enhanced interfacial chemistry on aqueous NaCl aerosols, Science, 288, 301–306, 2000.
Mack, J. and Bolton, J. R.: Photochemistry of nitrite and nitrate in aqueous solution: A review, J. Photochem. Photobiol. A. Chem., 101, 89–103, 1999.
Madronich, S.: Photodissociation in the atmosphere, 1. Actinic flux and the effect of ground reflection and clouds, J. Geophys. Res., 92, 9740–9752, 1987.
Marinoni, A., Laj, P., Sellegri, K., and Mailhot, G.: Cloud chemistry at the Puy de Dôme: variability and relationships with environmental factors, Atmos. Chem. Phys., 4, 715–728, 2004, http://www.atmos-chem-phys.net/4/715/2004/.
Mark, G., Korth, H.-G., Schuchmann, H.-P., and von Sonntag, C.: The photochemistry of aqueous nitrate ion revisited, J. Photochem. Photobiol. A. Chem., 101, 89–103, 1996.
Mazellier, P., Mailhot, G., and Bolte, M.: Photochemical behaviour of the iron(III)/2,6-

dimethylphenol system, New J. Chem., 21, 389–397, 1997.
Mayer, B. and Madronich, S.: Actinic flux and photolysis in water droplets: Mie calculations and geometrical optics limit, Atmos. Chem. Phys., 4, 2241–2250, 2004, http://www.atmos-chem-phys.net/4/2241/2004/.
Minero, C., Maurino, V., Bono, F., Pelizzetti, E., Marinoni, A., Mailhot, G., Carlotti, M. E., and Vione, D.: Effect of selected organic and inorganic snow and cloud components on the photochemical generation of nitrite by nitrate irradiation, Chemosphere, 68, 2111–2117, 2007.
Minofar, B., Jungwirth, P., Das, M. R., Kunz, W., and Mahiuddin, S. J.: Propensity of formate, acetate, benzoate, and phenolate for the aqueous solution/vapor interface: Surface tension measurements and molecular dynamics simulations, J. Phys. Chem. C., 111, 8242–8247, 2007.
Nissenson, P., Knox, C. J. H., Finlayson-Pitts, B. J., Phillips, L. F., and Dabdub, D.: Enhanced photolysis in aerosols: evidence for important surface effects, Phys. Chem. Chem. Phys., 8, 4700–4710, 2004.
Quan, X. and Fry, E. S.: Empirical equation for the index of refraction of seawater, Appl. Opt., 34, 3477–3480, 1995.
Ray, A. K. and Bhanti, D. D.: Effect of optical resonances on photochemical reactions in microdroplets, Appl. Opt., 36, 2663–2674, 1997.
Ruggaber, A., Dlugi, R., Bott, A., Forkel, R., Herrmann, H., and Jacobi, H.-W.: Modelling of radiation quantities and photolysis frequencies in the aqueous phase in the troposphere, Atmos. Environ., 31, 3137–3150, 1997.
Salvador, P., Curtis, J. E., Tobias, D. J., and Jungwirth, P.: Polarizability of the nitrate anion and its solvation at the air/water interface, Phys. Chem. Chem. Phys., 5, 3752–3757, 2003.
Takeda, K., Takedoi, H., Yamaji, S., Ohta, K., and Sakugawa, H.: Determination of hydroxyl radical photoproduction rates in natural waters, Anal. Sci., 20, 153–158, 2004.
Vacha, R., Slavicek, P., Mucha, M., Finlayson-Pitts, B. J., and Jungwirth, P.: Adsorption of atmospherically relevant gases at the air/water interface: Free energy profiles of aqueous solvation of N_2, O_2, O_3, OH, H_2O, HO_2, and H_2O_2, J. Phys. Chem. A., 108, 11573–11579, 2004.
Vacha, R., Jungwirth, P., Chenb, J., and Valsaraj, K.: Adsorption of polycyclic aromatic hydrocarbons at the air-water interface: Molecular dynamics simulations and experimental atmospheric observations, Phys. Chem. Chem. Phys., 8, 4461–4467, 2006.
Vione, D., Maurino, V., Minero, C., Pelizzetti, E., Harrison, M. A. J., Olariu, R. I., and Arsene,

ACPD
9, 13123–13153, 2009

C.: Photochemical reactions in the tropospheric aqueous phase and on particulate matter, Chem. Soc. Rev., 35, 441–453, 2006.
Vione, D., Minero, C., Hamraoui, A., and Privat, M.: Modelling photochemical reactions in atmospheric water droplets: An assessment of the importance of surface processes, Atmos. Environ., 41, 3303–3314, 2007.
Warneck, P.: The relative importance of various pathways for the oxidation of sulphur dioxide and nitrogen dioxide in sunlit continental fair weather clouds, Phys. Chem. Chem. Phys., 1, 5471–5483, 1999.
Warneck, P. and Wurzinger, C.: Product quantum yields for the 305-nm photodecomposition of NO_3^- in aqueous solution, J. Phys. Chem., 92, 6278–6283, 1988.
Wingen, L. M., Moskun, A. C., Johnson S. N., Thomas, J. L., Roeselova, M., Tobias, D. J., Kleinman, M. T., and Finlayson-Pitts, B. J.: Enhanced surface photochemistry in chloride-nitrate ion mixtures, Phys. Chem. Chem. Phys., 10, 5668–5677, 2008.
Winter, M. and Benjamin, I.: Photodissociation of ICN at the liquid/vapor interface of water, J. Chem. Phys., 121, 2253–2263, 2004.

Table 1. Photolysis quantum yields of $FeOH^{2+}$ at different wavelength values. The quantum yields that include the solvent-cage effect (solution bulk) are based on the data of Benkelberg and Warneck (1995). The quantum yields without the cage effect, relevant to the air-water interface, are based on the experimental results of this work and the additional hypothesis that the wavelength trend is similar to that of the bulk process (the one with the solvent-cage effect).

λ, nm	$\Phi(FeOH^{2+})$, solvent cage	$\Phi(FeOH^{2+})$, no solvent cage
290	0.21	1.0
300	0.16	1.0
310	0.14	1.0
320	0.12	0.85
330	0.11	0.74
340	0.10	0.63
350	0.07	0.45
360	0.04	0.18
370	0.04	0.18

ACPD

9, 13123–13153, 2009

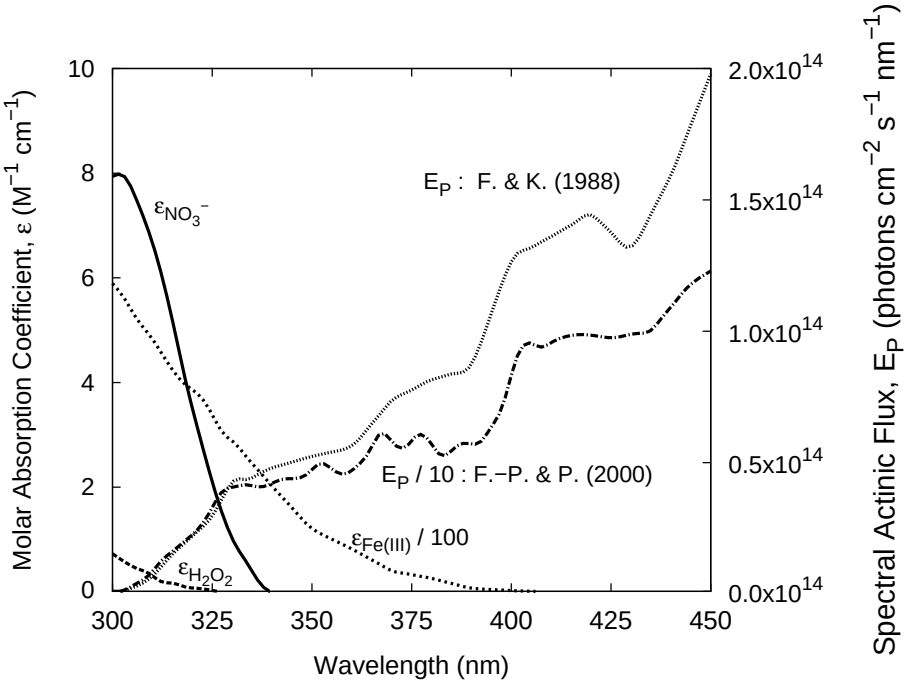

Fig. 1. Absorption spectra of nitrate, H_2O_2 and Fe(III), the latter at pH 2.5. Sunlight spectra according to Finlayson-Pitts and Pitts (2000) (F.-P. & P.) and Frank and Klöpffer (1988) (F. & K.).

ACPD
9, 13123–13153, 2009

CC BY

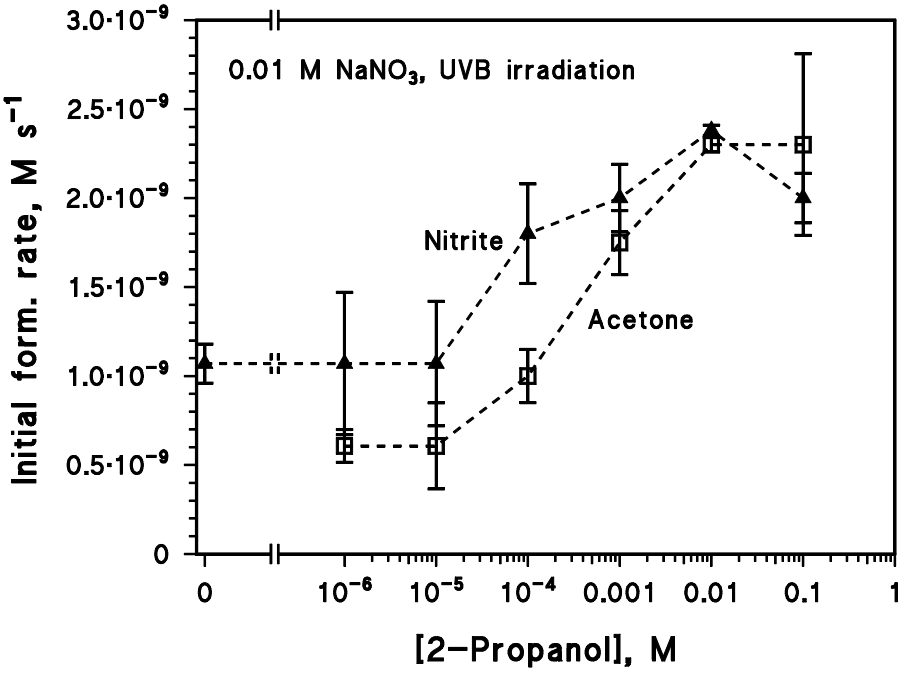

Fig. 2. Initial formation rates of nitrite and acetone as a function of the concentration of 2-propanol, upon UVB irradiation of 0.01 M $NaNO_3$. Note the logarithmic scale and the break in the X-axis.

ACPD
9, 13123–13153, 2009

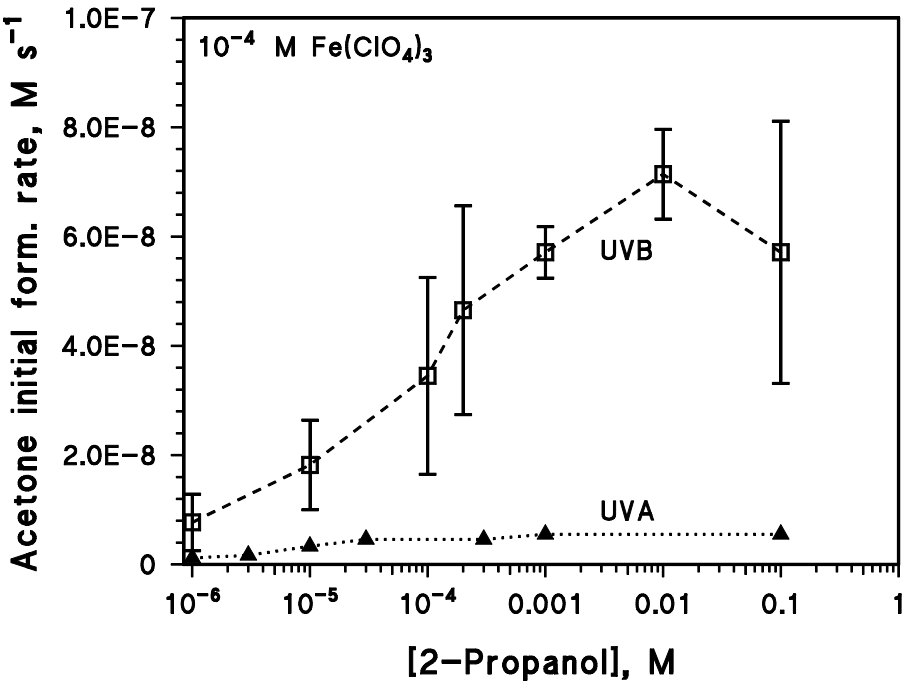

Fig. 3. Initial formation rates of acetone as a function of the concentration of 2-propanol, upon irradiation (UVB or UVA) of 0.1 mM $Fe(ClO_4)_3$. Note the logarithmic scale in the X-axis.

ACPD
9, 13123–13153, 2009

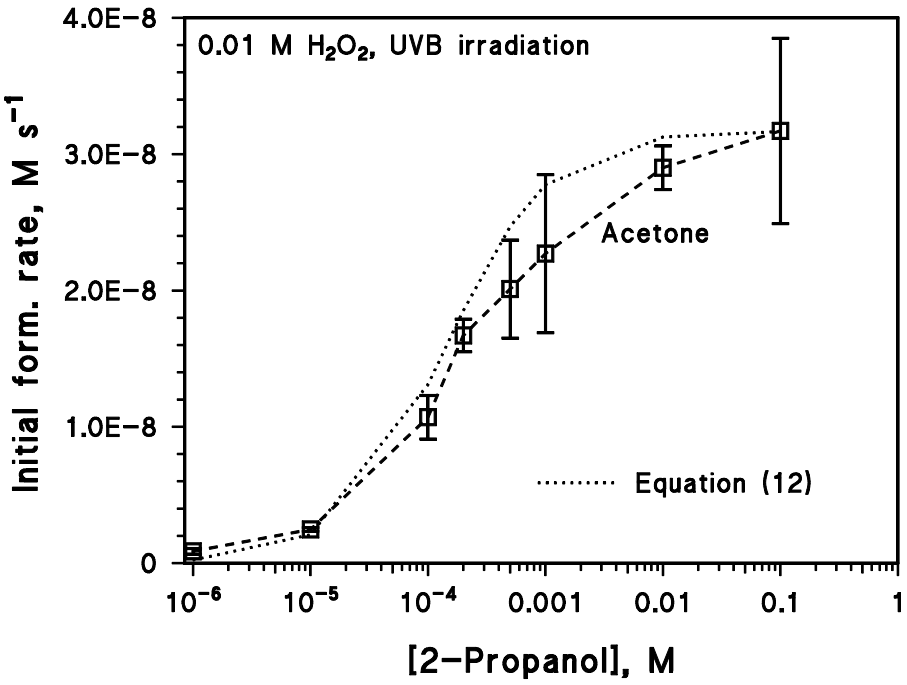

Fig. 4. Initial formation rates of acetone as a function of the concentration of 2-propanol, upon UVB irradiation of 0.01 M H_2O_2. Note the logarithmic scale in the X-axis.

ACPD
9, 13123–13153, 2009

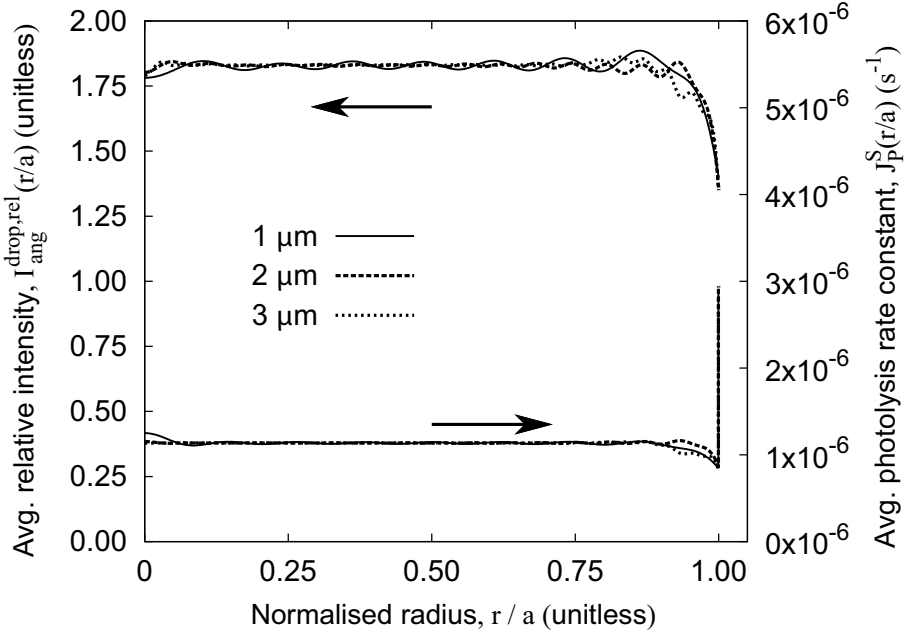

Fig. 5. The angle- and wavelength-averaged relative intensity ($I_{ang}^{drop,rel}$) and angle-averaged photolysis rate constant for nitrate ($J_P^{NO_3^-}$) as a function of normalized distance r/a from the droplet center. The water droplets of radius 1 μm, 2 μm, and 3 μm contain 10^{-4} M nitrate. The spectrum from Finlayson-Pitts and Pitts (2000) is used to calculate $I_{ang}^{drop,rel}$.

ACPD
9, 13123–13153, 2009

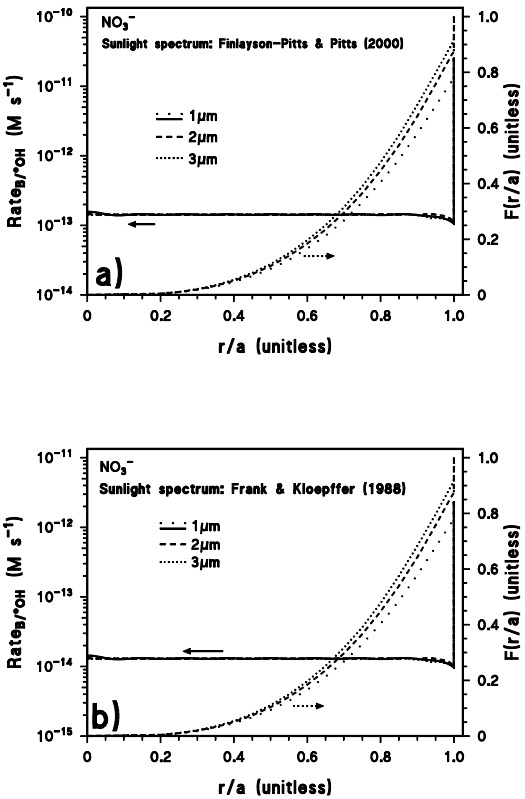

Fig. 6. Trends of $\text{Rate}_{B/\bullet\text{OH}}$ (see Eq. 18) and of $F(r/a)$ (Eq. 19) for 0.1 mM nitrate, as a function of the normalized distance r/a from the droplet center. The figure reports data for spherical droplets of radius a=1, 2 and 3 μm.

1. Sunlight spectrum as reported by Finlayson-Pitts and Pitts (2000).
2. Sunlight spectrum as reported by Klöpffer (1988).

ACPD
9, 13123–13153, 2009

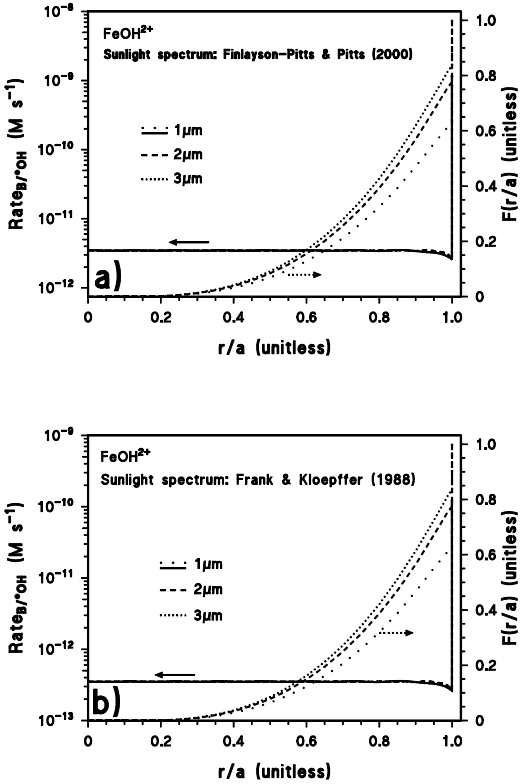

Fig. 7. Trends of $\text{Rate}_{B/\cdot\text{OH}}$ (see Eq. 18) and of $F(r/a)$ (Eq. 19) for 1 μM $FeOH^{2+}$, as a function of the normalized distance r/a from the droplet center. The figure reports data for spherical droplets of radius a=1, 2 and 3 μm.

1. Sunlight spectrum as reported by Finlayson-Pitts and Pitts (2000).
2. Sunlight spectrum as reported by Frank and Klöpffer (1988).

ACPD
9, 13123–13153, 2009

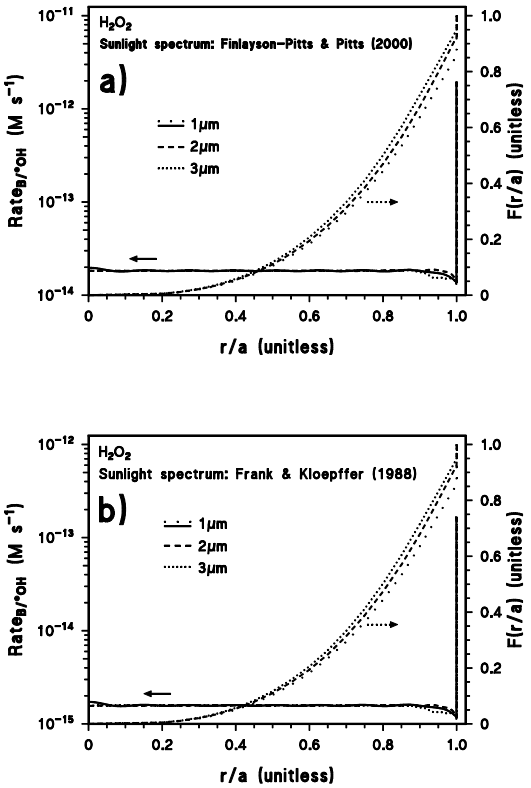

Fig. 8. Trends of $\text{Rate}_{B/^{\bullet}\text{OH}}$ (see Eq. 18) and of $F(r/a)$ (Eq. 19) for 10 μM H_2O_2, as a function of the normalized distance r/a from the droplet center. The figure reports data for spherical droplets of radius a=1, 2 and 3 μm.

1. Sunlight spectrum as reported by Finlayson-Pitts and Pitts (2000).
2. Sunlight spectrum as reported by Frank and Klöpffer (1988).

ACPD
9, 13123–13153, 2009